Wedge and gap plasmonic resonances in double nanoholes

Yuanyuan Chen, Abhay Kotnala, Li Yu, Jiasen Zhang, and Reuven Gordon

November 2015

This article was originally published at:

http://dx.doi.org/10.1364/OE.23.030227

Wedge and gap plasmonic resonances in double nanoholes

Yuanyuan Chen,[1,2] Abhay Kotnala,[2] Li Yu,[1] Jiasen Zhang,[3,4] and Reuven Gordon[2,*]

[1]*State Key Lab of Information Photonics and Optical Communications, Department of Science, Beijing University of posts and Telecommunications, Beijing 100876, China*
[2]*Department of Electrical and Computer Engineering, University of Victoria, Victoria, BC, V8W 3V6, Canada*
[3]*State Key Lab for Mesoscopic Physics, Department of Physics, Peking University, Beijing 100871, China*
[4]*Collaborative Innovation Center of Quantum Matter, Beijing, 100871, China*
[*]*rgordon@uvic.ca*

Abstract: We study the plasmonic resonances of double nanoholes (DNHs) in metal films. These apertures exhibit the usual gap-mode Fabry-Pérot resonances, where the zeroth order resonance is determined by the waveguide cut-off and the first order resonance shows sensitivity to the film thickness. An additional wedge resonance is observed, which is sensitive to the curvature of the cusps in the DNHs, analogous to the wedge modes of single wedges. While the gap mode intensity increases dramatically with decreasing gap-width, the wedge mode intensity saturates since its field enhancement arises from the curvature of the metal film, like cylindrical Sommerfeld waves. Experimental transmission spectra agree well with finite-difference time-domain simulations showing these separate resonances. The controlled design of these resonances is critical for applications including optical tweezers, nonlinear conversion, sensing and spectroscopy.

OCIS codes: (260.3910) Metal optics; (240.6680) Surface plasmons; (310.6628) Subwavelength structures, nanostructures; (160.4760) Optical properties; (260.5740) Resonance.

References and links

1. C. Genet and T. W. Ebbesen, "Light in tiny holes," Nature **445**(7123), 39–46 (2007).
2. F. J. Garcia-Vidal, L. Martín-Moreno, T. W. Ebbesen, and L. Kuipers, "Light passing through subwavelength apertures," Rev. Mod. Phys. **82**(1), 729–787 (2010).
3. T. H. Taminiau, R. J. Moerland, F. B. Segerink, L. Kuipers, and N. F. van Hulst, "λ/4 resonance of an optical monopole antenna probed by single molecule fluorescence," Nano Lett. **7**(1), 28–33 (2007).
4. T. S. van Zanten, M. J. Lopez-Bosque, and M. F. Garcia-Parajo, "Imaging individual proteins and nanodomains on intact cell membranes with a probe-based optical antenna," Small **6**(2), 270–275 (2010).
5. M. Melli, A. Polyakov, D. Gargas, C. Huynh, L. Scipioni, W. Bao, D. F. Ogletree, P. J. Schuck, S. Cabrini, and A. Weber-Bargioni, "Reaching the theoretical resonance quality factor limit in coaxial plasmonic nanoresonators fabricated by helium ion lithography," Nano Lett. **13**(6), 2687–2691 (2013).
6. A. Moreau, G. Granet, F. Baida, and D. Van Labeke, "Light transmission by subwavelength square coaxial aperture arrays in metallic films," Opt. Express **11**(10), 1131–1136 (2003).
7. E. X. Jin and X. Xu, "Plasmonic effects in near-field optical transmission enhancement through a single bowtie-shaped aperture," Appl. Phys. B **84**(1-2), 3–9 (2006).
8. E. X. Jin and X. Xu, "Enhanced optical near field from a bowtie aperture," Appl. Phys. Lett. **88**(15), 153110 (2006).
9. E. X. Jin and X. Xu, "Obtaining super resolution light spot using surface plasmon assisted sharp ridge nanoapertures," Appl. Phys. Lett. **86**(11), 111106 (2005).
10. X. Shi and L. Hesselink, "Ultrahigh light transmission through a C-shaped nanoapertures," J. Opt. Soc. Am. B **28**, 1320–1322 (2003).
11. J. A. Matteo, D. P. Fromm, Y. Yuen, P. J. Schuck, W. E. Moerner, and L. Hesselink, "Spectral analysis of strongly enhanced visible light transmission through single C-shaped nanoapertures," Appl. Phys. Lett. **85**(4), 648–650 (2004).
12. P. N. Melentiev, A. E. Afanasiev, A. A. Kuzin, A. S. Baturin, and V. I. Balykin, "Giant optical nonlinearity of a single plasmonic nanostructure," Opt. Express **21**(12), 13896–13905 (2013).

#248693 Received 27 Aug 2015; revised 3 Nov 2015; accepted 9 Nov 2015; published 11 Nov 2015

13. P. N. Melentiev, A. E. Afanasiev, A. A. Kuzin, A. S. Baturin, and V. I. Balykin, "Subwavelength light localization based on optical nonlinearity and light polarization," Opt. Lett. **38**(13), 2274–2276 (2013).
14. L. K. S. Kumar, A. Lesuffleur, M. C. Hughes, and R. Gordon, "Double nanohole apex-enhanced transmission in metal films," Appl. Phys. B **84**(1-2), 25–28 (2006).
15. T.-D. Onuta, M. Waegele, C. C. DuFort, W. L. Schaich, and B. Dragnea, "Optical field enhancement at cusps between adjacent nanoapertures," Nano Lett. **7**(3), 557–564 (2007).
16. M. L. Juan, M. Righini, and R. Quidant, "Plasmon nano-optical tweezers," Nat. Photonics **5**(6), 349–356 (2011).
17. A. A. Saleh and J. A. Dionne, "Toward efficient optical trapping of sub-10-nm particles with coaxial plasmonic apertures," Nano Lett. **12**(11), 5581–5586 (2012).
18. J. Berthelot, S. S. Aćimović, M. L. Juan, M. P. Kreuzer, J. Renger, and R. Quidant, "Three-dimensional manipulation with scanning near-field optical nanotweezers," Nat. Nanotechnol. **9**(4), 295–299 (2014).
19. A. Kotnala and R. Gordon, "Quantification of high-efficiency trapping of nanoparticles in a double nanohole optical tweezer," Nano Lett. **14**(2), 853–856 (2014).
20. J. A. H. van Nieuwstadt, M. Sandtke, R. H. Harmsen, F. B. Segerink, J. C. Prangsma, S. Enoch, and L. Kuipers, "Strong modification of the nonlinear optical response of metallic subwavelength hole arrays," Phys. Rev. Lett. **97**(14), 146102 (2006).
21. T. Xu, X. Jiao, G. P. Zhang, and S. Blair, "Second-harmonic emission from sub-wavelength apertures: Effects of aperture symmetry and lattice arrangement," Opt. Express **15**(21), 13894–13906 (2007).
22. A. Lesuffleur, L. K. S. Kumar, and R. Gordon, "Apex-enhanced second-harmonic generation by using double-hole arrays in a gold film," Phys. Rev. B **75**(4), 045423 (2007).
23. T. Rindzevicius, Y. Alaverdyan, A. Dahlin, F. Höök, D. S. Sutherland, and M. Käll, "Plasmonic sensing characteristics of single nanometric holes," Nano Lett. **5**(11), 2335–2339 (2005).
24. K. A. Tetz, L. Pang, and Y. Fainman, "High-resolution surface plasmon resonance sensor based on linewidth-optimized nanohole array transmittance," Opt. Lett. **31**(10), 1528–1530 (2006).
25. M. E. Stewart, C. R. Anderton, L. B. Thompson, J. Maria, S. K. Gray, J. A. Rogers, and R. G. Nuzzo, "Nanostructured plasmonic sensors," Chem. Rev. **108**(2), 494–521 (2008).
26. A. Kotnala, D. DePaoli, and R. Gordon, "Sensing nanoparticles using a double nanohole optical trap," Lab Chip **13**(20), 4142–4146 (2013).
27. L. Wang, S. M. Uppuluri, E. X. Jin, and X. Xu, "Nanolithography using high transmission nanoscale bowtie apertures," Nano Lett. **6**(3), 361–364 (2006).
28. N. Murphy-DuBay, L. Wang, and X. Xu, "Nanolithography using high transmission nanoscale ridge aperture probe," Appl. Phys., A Mater. Sci. Process. **93**(4), 881–884 (2008).
29. L. Wang and X. Xu, "High transmission nanoscale bowtie-shaped aperture probe for near-field optical imaging," Appl. Phys. Lett. **90**(26), 261105 (2007).
30. A. Weber-Bargioni, A. Schwartzberg, M. Cornaglia, A. Ismach, J. J. Urban, Y. Pang, R. Gordon, J. Bokor, M. B. Salmeron, D. F. Ogletree, P. Ashby, S. Cabrini, and P. J. Schuck, "Hyperspectral nanoscale imaging on dielectric substrates with coaxial optical antenna scan probes," Nano Lett. **11**(3), 1201–1207 (2011).
31. A. G. Brolo, E. Arctander, R. Gordon, B. Leathem, and K. L. Kavanagh, "Nanohole-enhanced raman scattering," Nano Lett. **4**(10), 2015–2018 (2004).
32. Y. Liu and S. Blair, "Fluorescence enhancement from an array of subwavelength metal apertures," Opt. Lett. **28**(7), 507–509 (2003).
33. G. Lu, W. Li, T. Zhang, S. Yue, J. Liu, L. Hou, Z. Li, and Q. Gong, "Plasmonic-enhanced molecular fluorescence within isolated bowtie nano-apertures," ACS Nano **6**(2), 1438–1448 (2012).
34. Q. Min, M. J. L. Santos, E. M. Girotto, A. G. Brolo, and R. Gordon, "Localized Raman enhancement from a double-hole nanostructure in a metal film," J. Phys. Chem. C **112**(39), 15098–15101 (2008).
35. M. L. Juan, R. Gordon, Y. Pang, F. Eftekhari, and R. Quidant, "Self-induced back-action optical trapping of dielectric nanoparticles," Nat. Phys. **5**(12), 915–919 (2009).
36. L. Neumann, Y. Pang, A. Houyou, M. L. Juan, R. Gordon, and N. F. van Hulst, "Extraordinary optical transmission brightens near-field fiber probe," Nano Lett. **11**(2), 355–360 (2011).
37. H. Rigneault, J. Capoulade, J. Dintinger, J. Wenger, N. Bonod, E. Popov, T. W. Ebbesen, and P. F. Lenne, "Enhancement of single-molecule fluorescence detection in subwavelength apertures," Phys. Rev. Lett. **95**(11), 117401 (2005).
38. Y. Pang and R. Gordon, "Optical trapping of 12 nm dielectric spheres using double-nanoholes in a gold film," Nano Lett. **11**(9), 3763–3767 (2011).
39. Y. Pang and R. Gordon, "Optical trapping of a single protein," Nano Lett. **12**(1), 402–406 (2012).
40. T. Matsui, A. Agrawal, A. Nahata, and Z. V. Vardeny, "Transmission resonances through aperiodic arrays of subwavelength apertures," Nature **446**(7135), 517–521 (2007).
41. H. Cao and A. Nahata, "Influence of aperture shape on the transmission properties of a periodic array of subwavelength apertures," Opt. Express **12**(16), 3664–3672 (2004).
42. M. J. Lockyear, A. P. Hibbins, J. R. Sambles, and C. R. Lawrence, "Surface-topography-induced enhanced transmission and directivity of microwave radiation through a subwavelength circular metal aperture," Appl. Phys. Lett. **84**(12), 2040 (2004).
43. Y. Chen, L. Yu, J. Zhang, and R. Gordon, "Effective wavelength scaling of rectangular aperture antennas," Opt. Express **23**(8), 10385–10395 (2015).

#248693 Received 27 Aug 2015; revised 3 Nov 2015; accepted 9 Nov 2015; published 11 Nov 2015

44. H. Guo, T. P. Meyrath, T. Zentgraf, N. Liu, L. Fu, H. Schweizer, and H. Giessen, "Optical resonances of bowtie slot antennas and their geometry and material dependence," Opt. Express **16**(11), 7756–7766 (2008).
45. I. A. Ibrahim, M. Mivelle, T. Grosjean, J. T. Allegre, G. W. Burr, and F. I. Baida, "Bowtie-shaped nanoaperture: a modal study," Opt. Lett. **35**(14), 2448–2450 (2010).
46. E. Feigenbaum and M. Orenstein, "Nano plasmon polariton modes of a wedge cross section metal waveguide," Opt. Express **14**(19), 8779–8784 (2006).
47. E. Feigenbaum and M. Orenstein, "Modeling of complementary (void) plasmon waveguiding," J. Lightwave Technol. **25**(9), 2547–2562 (2007).
48. E. Moreno, S. G. Rodrigo, S. I. Bozhevolnyi, L. Martín-Moreno, and F. J. García-Vidal, "Guiding and focusing of electromagnetic fields with wedge plasmon polaritons," Phys. Rev. Lett. **100**(2), 023901 (2008).
49. L. Wang and X. Xu, "Spectral resonance of nanoscale bowtie apertures in visible wavelength," Appl. Phys., A Mater. Sci. Process. **89**(2), 293–297 (2007).
50. FDTD Solutions, from Lumerical Solutions, Inc., Canada.
51. D. K. Gramotnev, A. Pors, M. Willatzen, and S. I. Bozhevolnyi, "Gap-plasmon nanonantennas and bowtie resonators," Phys. Rev. B **85**(4), 04543 (2012).
52. T.-I. Jeon, J. Zhang, and D. Grischkowsky, "THz sommerfeld wave propagation on a single metal wire," Appl. Phys. Lett. **86**(16), 161904 (2005).

1. Introduction

Nanoapertures in metallic thin films have shown the ability to significantly enhance optical fields in the nanoscale region that they define at the resonance frequency [1,2]. Different nanoaperture shapes, such as tip-on-aperture [3,4], coaxial aperture [5,6], bowtie-shaped aperture [7–9], C-shaped aperture [10,11], split-hole resonator [12,13] and double-nanohole (DNH) [14,15], have been used to increase both the power transmission and the effective field confinement for applications in optical tweezers [16–19], nonlinear optics [20–22], sensing [23–26], nanolithography [27,28], near-field probes [29,30] and surface enhanced Raman spectroscopy [31–34]. For example, bowtie nanoaperture antennas (BNAs) provide a confined spot with an intense local field and broadband response in the visible regime [8,9] and have been successfully used as nanometer-sized light sources for nanolithography [27] and high throughput near-field probes [29]. For optical trapping, nanoapertures provide efficient trapping due to the strong perturbation of the nanoparticle to the local electromagnetic environment in the aperture [35]. The nanoaperture approach provides a high signal-to-noise ratio due to the background free operation from the aperture, as well as a trivial detection approach [36,37]. Our lab has already shown the trapping of particles of 12 nm in size [38] and even the single proteins [39] using a double nanohole (DNH) optical aperture. For these applications, we aim to understand the role of aperture geometry on the resonant transmission and near-field properties.

Many works have studied how the resonance condition depends on the size and geometry of the nanoapertures [40–43]. It is important to design the geometry of the nanoaperture properly to enhance transmission and to produce a bright nanoscale spot. Several papers have researched the optical resonances of BNAs with dependence on geometry and metal properties to provide a guide for the design and optimization of BNAs for a variety of applications [44,45]. In the past, two types of resonances were identified: a plasmonic resonance and a Fabry-Pérot (FP) like resonance. Of course, the plasmonic resonance may be considered as the zeroth order FP resonance.

Here we perform a similar analysis for the DNH and identify an additional wedge resonance that comes from the curvature of the cusps in the DNH. Wedge modes have been studied in the past for single curved edges [46–48]. The wedge resonance peaks may have also been observed in the spectrum of the bowtie apertures [49]; however, the particular identification of that mode as a wedge mode was not presented. In addition, most previous theoretical works used pointed or flat edges, and so the wedge mode, which comes from curvature, was not apparent. We perform finite-difference time-domain (FDTD) simulations to investigate the usual gap-mode FP resonances and the wedge resonance not studied in those past works on apertures. Furthermore, we measure the transmission spectra of various apertures to identify these resonances in actual structures, with good agreement to FDTD

#248693 Received 27 Aug 2015; revised 3 Nov 2015; accepted 9 Nov 2015; published 11 Nov 2015

modeling. Past works on optical tweezers have investigated the role of the resonant transmission modes on the trapping performance [16–18]; therefore, it is important to identify the modes present in the aperture and to quantify their influence on trapping. Of particular note, since the wedge modes are tightly confined to the wedge, they are good candidates for trapping experiments; however, this remains to be investigated in future works.

2. Plasmonic resonances of DNHs

DNHs are composed of two circular apertures in a metal film separated by a small opening, as shown schematically in Fig. 1(a). Here, the gold film is evaporated on a glass substrate and studied in water (for trapping applications). The geometry of the DNH is defined by the thickness of the metal, T, the diameter of the circular aperture, D, the distance between the two circular apertures, L (the center-to-center separation), the curvature of the cusps, C, and width, W, of the gap. The system is illuminated by a normally incident plane wave with linear polarization along the x direction, as shown in Fig. 1(a).

To analyze the resonances of the DNHs, we use FDTD numerical calculations [50]. In the simulation, the source used is a Total Field Scattered Field (TFSF). Convergence was ensured by reducing the grid-size and extending the artificial Perfectly Matched Layer (PML) boundaries. The smallest grid-size attempted was 1 nm. The metal has relative permittivity that was modeled according to the Drude theory, which offers a good correspondence to the measured data over a broad spectral range and is given by

$$\varepsilon_m = \varepsilon_\infty - \frac{{\omega_p}^2}{\omega^2 + i\gamma\omega} \tag{1}$$

where ε_∞ is the infinite frequency limit of the dielectric function, ω_p is the plasma frequency and $\gamma = \frac{1}{\tau}$ is the electron scattering rate. For gold, $\varepsilon_\infty \approx 11$, $\omega_p = 1.37\text{e}16$ Hz and $\gamma = 1.05\text{e}14$ Hz.

Figure 1(b) shows a typical transmission spectrum of a DNH structure. We set T = 150 nm, D = 120 nm, L = 130 nm, W = 30 nm and C = 0.035. The index of the substrate and the water is 1.51 and 1.33. One can see three transmission resonances in the full wavelength regime. To obtain physical insight into these resonances, the electric field intensity distributions at the resonant wavelengths are shown in Figs. 1(c) and 1(d) (x-z and x-y planes). According to Fig. 1(c), one can clearly see a uniform electric field intensity distribution of the zeroth order FP mode (FP_0) along the metal thickness for the resonance at the wavelength 1323 nm (top of Fig. 1(c)). One node appears near the middle of the cavity for the FP_1 resonance at the wavelength 798 nm (bottom of Fig. 1(c)). Similar resonance peaks have already been reported in the transmission spectrum of BNAs [44,45]. Since the field intensity is largest and confined in the gap, we refer to these two FP resonances as gap mode FP resonances [51]. In addition to these previously studied resonances, we also observed an interesting resonance at the wavelength of 1182 nm. In contrast to the gap mode FP resonance, the field intensity distribution of this resonance peak shows enhancement around the edge of the gap and inside the metal, as shown in Fig. 1(d). Since this distribution is similar to the wedge plasmon waveguides [46–48], we refer to it as a wedge resonance.

#248693 Received 27 Aug 2015; revised 3 Nov 2015; accepted 9 Nov 2015; published 11 Nov 2015

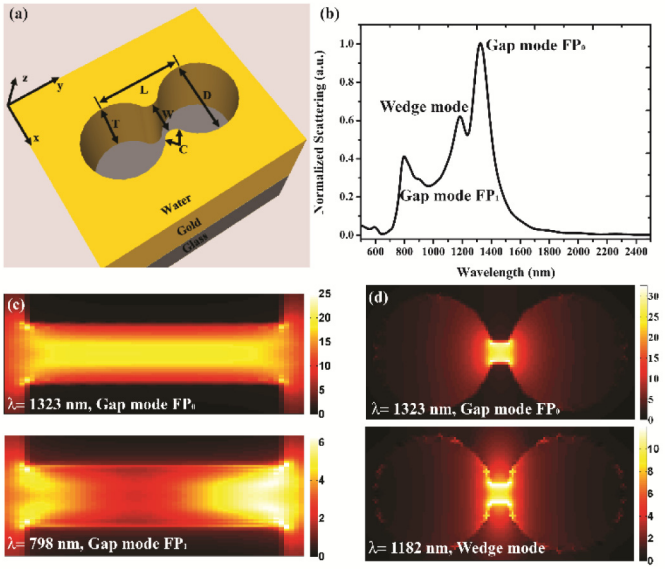

Fig. 1. (a) Schematic view of a double nanohole structure in metal film. The geometry of the DNH is defined by the thickness of the metal, T, the diameter of the circular aperture, D, the distance between the two circular apertures, L (the center-to-center separation), the curvature, C and width, W of the gap. (b) The transmission spectra of DNH aperture with T = 150 nm, D = 120 nm, L = 130 nm, W = 30 nm and C = 0.035. (c) Electricfield intensity distributions in the x–z plane for λ = 1323 nm, λ = 798 nm. (d) Electric field intensity distributions in the x–y plane for λ = 1323 nm, λ = 1182 nm.

3. Gap mode FP resonance and wedge resonance

The FP resonance peak can be found from:

$$\lambda = \frac{2n_{eff}T}{m} + R \qquad (2)$$

where n_{eff} is the effective refractive index of the aperture mode, m is an integer and R originates from the phase of reflection. Figure 2(a) shows the dependence of the gap mode FP_1 resonance on film thickness (T). The wavelength of the gap mode FP_1 resonance shifted from 732 nm to 913 nm when the thickness of the gold was varied from 100 nm to 200 nm. The gap mode FP resonance in the long wavelength range has a uniform electric field intensity distribution of the FP_0 mode along the metal thickness. In fact, its wavelength is almost independent of the metal thickness as shown in the Fig. 2(a).

The gap mode FP_0 resonance occurs close to the cutoff wavelength that depends on the geometry of the aperture and not the film thickness. This result is confirmed by simulations using a mode source in FDTD to determine where the effective index is nearly zero (i.e., the cut-off) as shown in Fig. 2(a). From the electric field distribution and phase distribution shown in the Fig. 2(b), it is clear that the electric field of gap mode FP_0 resonance is mainly confined in the aperture and the maxima of the amplitude of the field appears in the gap of the DNH structure. The phase of the field is uniform inside the DNH.

Similarly, the wedge mode resonance occurs close to its cut-off value, so there is little sensitivity to film thickness as shown in Fig. 2(a). This implies that it is the zeroth order FP resonance of the wedge mode. Different from the gap mode FP resonances, the wedge resonance is very sensitive to the change of the curvature of the gap as shown in Fig. 2(c). The small change of the curvature of the gap from 0.025 to 0.035 cause an obvious shift in the

#248693 Received 27 Aug 2015; revised 3 Nov 2015; accepted 9 Nov 2015; published 11 Nov 2015

wedge resonance. Figure 2(d) plots the electric field distribution and phase distribution in the x–z plane for wedge resonance. We find the maxima of the amplitude of the electric field is around the edges of the wedge and the electric field appears in the middle of the cusps (in the metal). The phase of the response field increases in the wedge, rather than in the gap, which is different with the gap mode FP_0 resonance shown in Fig. 2(b).

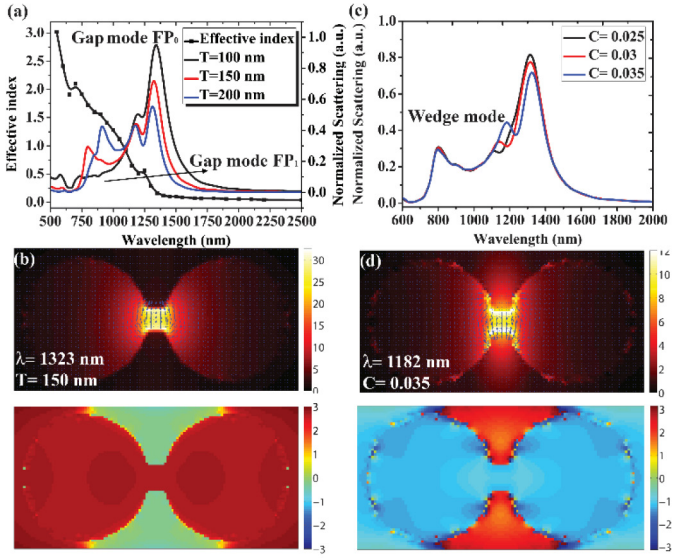

Fig. 2. (a) The black line-symbol represents the effective index as function of the wavelength for DNH with T = 150 nm, D = 120 nm, L = 130 nm, W = 30 nm and C = 0.035. The black, red and blue lines represent the transmission spectra of DNH apertures of three different thickness with D = 120 nm, L = 130 nm, W = 30 nm and C = 0.035. (b) The electric field distribution and phase distribution in the x–z plane for λ = 1323 nm, and T = 150 nm. (c) The transmission spectra of DNH apertures of three different curvature with T = 150 nm, D = 120 nm, L = 130 nm, W = 30 nm. (d) The electric field distribution and phase distribution in the x–z plane for λ = 1182 nm and C = 0.035.

4. Resonance dependence on other geometric parameters

It is well known that light transmission through metallic apertures has strong size dependence [1,2,41–44]. To analyze the optical response of DNHs with different geometry sizes, influences of the diameter of the DNHs are first to come up with. Figure 3(a) plots the transmission spectra of DNHs with aperture diameter changing from 100 nm to 160 nm. It is clear that the resonant electric intensity is increasing and the resonance spectra is broadened with the increase of aperture diameter. The plot in Fig. 3(b) shows the wavelengths of the gap mode FP_0 resonance, wedge resonance and gap mode FP_1 resonance as functions of aperture diameter. We can see the gap mode FP_0 resonances are very sensitive to the change of the aperture diameter. This is consistent with the point that the gap mode FP_0 resonance is close to the cutoff wavelength that depends on the size of the aperture. Due to the change of the diameter, the curvature of the gap is also adjusted, which leads the wedge resonant peak move to the longer wavelength. As show in Fig. 3(b), the wedge resonance is more sensitive to the change of the diameter. Thus, the wedge resonant peak is sometimes cutoff by the aperture and will disappear as shown in Fig. 3(a) (top figure and larger diameter apertures not shown). The slight change of the gap mode FP_1 resonance is related with the effective refractive index (n_{eff}), which is a parameter that depends on structure geometry.

#248693 Received 27 Aug 2015; revised 3 Nov 2015; accepted 9 Nov 2015; published 11 Nov 2015

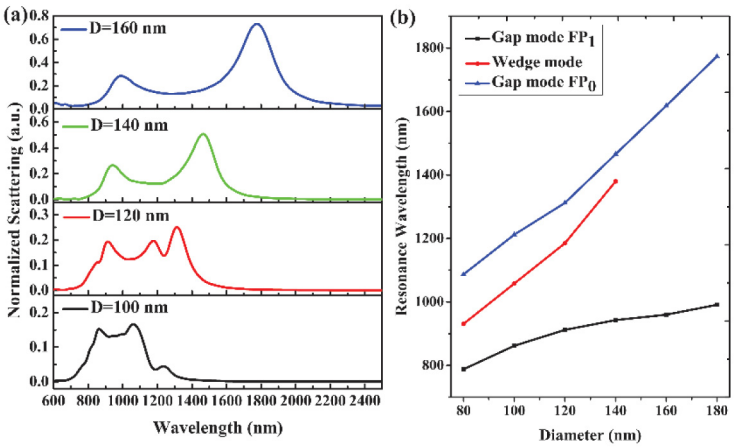

Fig. 3. (a) The transmission spectra of DNHs with aperture diameter changing from 100 nm to 160 nm and T = 200 nm, L = 130 nm, W = 30 nm and C = 0.035 is fixed. (b) The resonance wavelengths of gap, wedge and FP resonances as function of the aperture diameter of the DNHs.

Given the diameter-dependence, we take a typical diameter of 120 nm in the following discussion to investigate the influence of gap size (width and length) on the spectral responses and the field enhancement at resonance, as shown in Fig. 4. Figure 4(a) shows that increasing the gap width will cause all the resonance to blue-shift. For the smaller gap width, the resonances are more sensitive to the change of the width. Increase of the gap width leads to the exponential attenuation of field enhancement for the gap mode FP resonances as shown in Fig. 4(b). An interesting finding is that the field enhancement of the wedge mode is not as sensitive on the gap width for larger gaps because the mode confinement comes from the curvature of the metal (like the confinement of a Sommerfeld wave on a metal wire [52]). For the three kinds of resonance, the gap mode FP_0 one produces the maximum field enhancement for the narrow gap with width smaller than 20 nm. Figures 4(c) and 4(d) reveal another series of spectral responses and field enhancement with different nanohole (NH) separation (the center-to-center separation, L). Increasing the NH separation, the gap mode FP_0 resonance shifts to the red linearly, while the electric field enhancement is almost constant. The wedge mode resonance, which is mainly effected by the curvature of the metal, remains nearly unchanged, while the field enhancement decreases with the NH separation becoming longer. Thus, for the DNH with a long gap, the wedge mode peak will disappear.

#248693 Received 27 Aug 2015; revised 3 Nov 2015; accepted 9 Nov 2015; published 11 Nov 2015

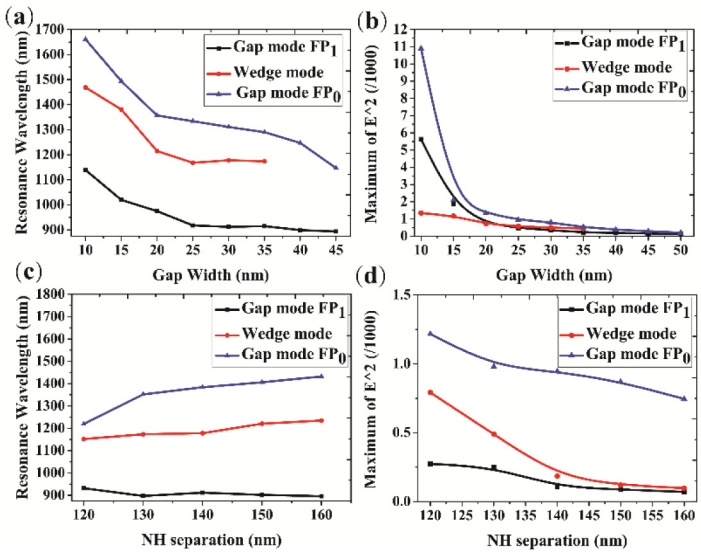

Fig. 4. (a) The resonance wavelengths of gap mode FP_0, wedge and gap mode FP_1 resonances as functions of the gap width, W of the DNH. (b) The maximum field intensity (normalized to incident field intensity) at resonance as a function of the gap width of the DNH. (c) The resonance wavelengths of gap mode FP_0, wedge and gap mode FP_1 resonances as functions of the NH separation, L of the DNH. (d) The maximum field intensity (normalized to incident field intensity) at resonance as a function of the NH separation of the DNH.

5. Experiment

The DNHs were fabricated in a 100 nm thick Au film on a glass substrate (with a 5 nm titanium adhesion layer) by focused ion beam milling. The DNHs were placed in the water by using a microwell to reproduce the trapping experimental configuration [19,26]. According to the scanning electron microscope (SEM) images shown in Fig. 5(a) and 5(d), the diameter of the DHNs D = 120 nm/178 nm, the gap width W = 45 nm/50 nm and the NH separation L = 145 nm/205 nm. Optical characterization was implemented using transmission spectroscopy. A broadband white light source (Fianium SC400) was focused and polarized perpendicular to the DNH axis. It normally illuminated the sample from the substrate. The transmitted light was collected by a microscope objective (100x/0.9NA) and sent into two spectrometers (Ocean Optics QE65000 and Ocean Optics USB2000), which can jointly detect the wavelength ranging from 500 nm to 1750 nm. One aperture was placed in the image plane to ensure that only the light transmitting through the DNH can enter the spectrometer. The measured extinction spectra are shown in Figs. 5(b) and 5(e). The red curves represent the measurement from the experiment. The black curves represent the simulation result, where we import the corresponding structures directly into FDTD using the image importing utility from the SEM images.

We find that the simulated spectral curves follow the same trend as the experimental results: there are two gap mode resonant peaks (FP_1 and FP_0 resonance) for each DNH, and there is a wedge mode peak as seen from the trend of the calculated curve. The numerical calculation and measurement also predict a red shift when the DNH size increases. Considering that there are subtle differences between the experiment and the simulations (e.g., the focusing of the beams and finite collection angles, the sloped edges with milling the gold, the varying material parameters), we believe that the agreement in terms of peak position and relative amplitude is good. FDTD simulated field intensity distribution of the gap mode FP_0 resonance and the wedge resonance in the x-y plane are shown in Figs. 5(c) and 5(f). The differences of the electric field enhancement between the gap mode FP_0 resonance and the

#248693 Received 27 Aug 2015; revised 3 Nov 2015; accepted 9 Nov 2015; published 11 Nov 2015

wedge resonance are obvious, which confirms the existence of the two kind of modes, the gap mode and the wedge mode in the experimental results.

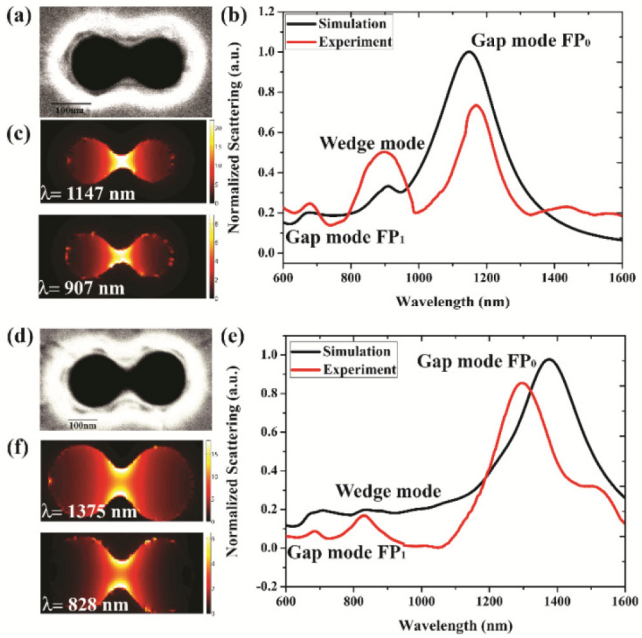

Fig. 5. (a) The scanning electron microscope image of a DNH in a gold film on glass substrate. The thickness of the gold is 100 nm, the diameter of the DHN D = 120 nm, the gap width W = 45 nm and the NH separation L = 145 nm. (b) The measured far-field transmission spectra of the DNH in (a) for normal light incidence. (c) FDTD simulated field intensity distribution of the DNH in (a) at the excitation wavelengths of 1147 nm and 907 nm. (d) The scanning electron microscope image of a DNH with the thickness of the gold T = 100 nm the diameter of the DHN D = 178 nm, the gap width W = 50 nm and the NH separation L = 205 nm. (e) The measured far-field transmission spectra of the DNH in (d) for normal light incidence. (f) FDTD simulated field intensity distribution of the DNH in (d) at the excitation wavelengths of 1375 nm and 828 nm.

6. Conclusion

In summary, we have studied the gap and wedge mode resonances of a double-nanohole in a metal film in the visible to near infrared spectral range. The gap mode FP_0 resonance depends on the cut-off of the gap mode and is nearly independent of the metal film thickness. The electric field enhancement of the gap mode FP_0 resonance is sensitive to the gap width of the DNH and shows an approximately exponential increase with decreasing gap width. The wedge resonance is mainly influenced by the curvature of the cusps in the DNH and the electric field enhancement does not vary significantly when decreasing the gap size (in contrast to the gap mode). The gap mode FP_1 resonance is sensitive to the film thickness and appears at shorter wavelengths as compared to the gap mode FP_0 and wedge resonance. Depending on the wavelength range, one can effectively tune the nanoaperture operating wavelength of each of the modes by varying the aperture size, cusp curvature and film thickness, which gives great flexibility for many applications including nonlinear mixing, Raman spectroscopy and optical trapping.

#248693 Received 27 Aug 2015; revised 3 Nov 2015; accepted 9 Nov 2015; published 11 Nov 2015

Acknowledgments

This work was supported by the Natural Sciences and Engineering Research Council of Canada (NSERC) Discovery Grant, the National Natural Science Foundation of China (NSFC) under Grant Nos. 11374041, 61377050, 11574011 and 11574035, the BUPT Excellent Ph.D. Students Foundation under Grant Nos. CX201324 and the Fund of State Key Laboratory of Information Photonics and Optical Communications of Beijing University of Posts and Telecommunications.

#248693 Received 27 Aug 2015; revised 3 Nov 2015; accepted 9 Nov 2015; published 11 Nov 2015